JACS
JOURNAL OF THE AMERICAN CHEMICAL SOCIETY

Communication

pubs.acs.org/JACS

Decoupling Mechanisms of Platinum Deposition on Colloidal Gold Nanoparticle Substrates

Patrick J. Straney,[†] Lauren E. Marbella,[†] Christopher M. Andolina,[†] Noel T. Nuhfer,[‡] and Jill E. Millstone*[,†]

[†]Department of Chemistry, University of Pittsburgh, Pittsburgh, Pennsylvania 15260, United States

[‡]Department of Materials Science and Engineering, Carnegie Mellon University, Pittsburgh, Pennsylvania 15213, United States

Supporting Information

ABSTRACT: Nanoscale platinum materials are essential components in many technologies, including catalytic converters and fuel cells. Combining Pt with other metals can enhance its performance and/or decrease the cost of the technology, and a wide range of strategies have been developed to capitalize on these advantages. However, wet chemical synthesis of Pt-containing nanoparticles (NPs) is challenging due to the diverse metal segregation and metal−metal redox processes possible under closely related experimental conditions. Here, we elucidate the relationship between Pt(IV) speciation and the formation of well-known NP motifs, including frame-like and core−shell morphologies, in Au−Pt systems. We leverage insights gained from these studies to induce a controlled transition from redox- to surface chemistry-mediated growth pathways, resulting in the formation of Pt NPs in epitaxial contact and linear alignment along a gold nanoprism substrate. Mechanistic investigations using a combination of electron microscopy and ^{195}Pt NMR spectroscopy identify Pt(IV) speciation as a crucial parameter for understanding and controlling the formation of Pt-containing NPs. Combined, these findings point toward fully bottom-up methods for deposition and organization of NPs on colloidal plasmonic substrates.

Multimetallic nanostructures are an exciting class of materials because they may exhibit new or enhanced properties when compared to their monometallic counterparts.[1−3] A myriad of multimetallic materials have been reported and are synthetically accessible in various sizes, shapes, and compositions.[3,4] Of the many different target compositions, platinum is a frequent component because of its broad utility in heterogeneous catalysis.[2,5] Forming multimetallic systems that include Pt can both enhance catalytic activity[6−8] and offer routes to reduce catalyst cost.[9,10]

One widely studied strategy for preparing Pt-containing nanoparticles (NPs) uses seed-mediated techniques.[11] In these syntheses, a monometallic NP substrate is used as a template for the addition of a second metal. When a second metal is introduced, it may deposit onto, alloy with, and/or oxidize the existing particle substrate.[12−15] However, the same metal combination may exhibit one or all of these reaction pathways—even within a single synthesis. The use of Pt in these syntheses is particularly challenging (in both seed-mediated and other wet chemical preparation strategies) because of the rapid hydrolysis of common precursors (e.g., $[PtCl_6]^{2-}$) and the sensitivity of these reactions to time, temperature, light, concentration, and pH.[16−18] In Pt-containing multimetallic NP syntheses, this speciation may result in similar reaction conditions giving rise to markedly different morphologies. For example, galvanic replacement reactions (GRRs) and core−shell products are both observed, sometimes in the same synthesis.[19−22]

Here, we use a combination of ^{195}Pt NMR and electron microscopy techniques to study the deposition of Pt onto Au NP substrates. These studies demonstrate the critical role of initial Pt(IV) speciation in final NP outcomes. We then use insights gained from these studies to induce a controllable transition from surface chemistry- to redox-mediated growth pathways, which yields a suite of alloyed and multicomponent Au−Pt NPs. In a typical reaction, Au nanoprism substrates (edge length = 150 ± 25 nm, thickness = 8 ± 2 nm) were synthesized using literature protocols (see Supporting Information (SI) for full synthesis details).[23] Reduction of aqueous H_2PtCl_6 (chloroplatinic acid, CPA) by ascorbic acid (AA) in the presence of purified Au nanoprisms (but in the absence of added surfactants or other reagents) led to heterogeneous nucleation of NP islands arranged linearly across the Au prism surface (diameter = 3.5 ± 0.4 nm; Figure 1).

The morphology, crystal structure, and composition of the resulting particles were analyzed using electron microscopy techniques. High-resolution transmission electron microscopy (HRTEM) and selected area electron diffraction (SAED) images indicate that the islands are in epitaxial contact with the underlying prism substrate. This observation is important in order to understand Pt NP formation. Epitaxial growth indicates that islands form from the particle substrate via a heterogeneous nucleation process as opposed to homogeneous nucleation and subsequent deposition onto the nanoprism. These observations are also consistent with time-dependent studies of island growth (*vide infra* and SI, Figures S2 and S3).

The composition of the resulting particles was analyzed by scanning transmission electron microscopy-energy dispersive X-ray spectroscopy (STEM-EDS). Here, composition is reported as the intensity of the M edges of Au and Pt from a line scan obtained along the altitude of the triangle (Figure S4). The

Received: May 1, 2014
Published: May 23, 2014

   dx.doi.org/10.1021/ja504294p | *J. Am. Chem. Soc.* 2014, 136, 7873−7876

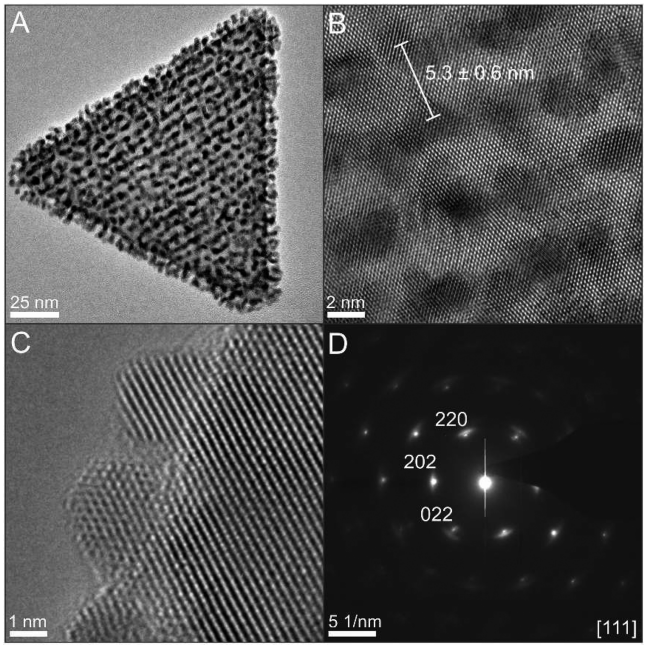

Figure 1. HRTEM images of Pt island-functionalized Au nanoprism (A), regular spacing between Pt island rows (B), and pendant Pt NPs (C). SAED pattern (D) indicates epitaxial alignment between Pt and Au components.

average distance between element peaks in the line scan correlates well with the analysis of island spacing from both scanning electron microscopy (SEM) and bright-field TEM images (5.4 ± 1.8 and 5.6 ± 1.8 nm for the Au-M and Pt-M edges, respectively). Interestingly, the Au and Pt signals rise coincidently, as opposed to a constant Au signal, expected from the flat top facet of the nanoprism substrate.[24,25] This modulation in both Au and Pt intensity is consistent with the formation of island structures, where changes in thickness of the material interacting with the beam path combined with the similar edge energies of Au and Pt create a coincidence in signal intensity and obscure quantitative comparison. Using additional STEM-EDS analysis of Pt islands pendant on the nanoprism side facets (Figure S5), we find that the islands are composed primarily of Pt, indicating little to no metal mixing between the Au substrate and the attached Pt NPs. Both the formation of Pt islands (Volmer–Weber growth, as opposed to oxidation or core–shell products) and the low degree of metal mixing are consistent with observations in bulk and thin-film Au–Pt systems,[26,27] and Pt deposition on NPs has been observed to form related "dendritic" structures.[28,29]

Optical features of the resulting particle products were analyzed by UV-vis-NIR absorption spectroscopy and compared with the optical properties of pure Au nanoprisms. After Pt deposition, the localized surface plasmon resonance (LSPR) of the nanoprisms ($\lambda_{max} \approx 1260$ nm) broadens and exhibits a hypsochromic shift that ranges from 10 to 150 nm, depending on the amount of Pt deposited (Figure S6). These optical features are consistent with damping of the Au LSPR either from dielectric effects or charge transfer between the two materials.[28,30] Extent of LSPR damping is found to correlate with the density of islands on the nanoprism surface, where increased island density leads to decreased LSPR intensity and increased spectral breadth. Island density was controlled using classic NP synthesis strategies, where keeping the metal ion-to-reducing agent ratio constant, we increased the total amount of metal ion and reducing agent used in the synthesis, which led to a larger quantity of similarly sized particles. (This result can also be achieved by keeping the total amount of metal ion and reducing agent constant and decreasing the amount of nanoprism seeds.) Island growth was found to occur relatively rapidly, beginning with formation on the nanoprism side facets, and reaching complete coverage of the broad triangular faces approximately 1 h after synthesis (Figures S2 and S3).

With initial particle characterization in hand, we investigate two key aspects of the resulting particle morphology: (1) the observation of Pt deposition onto the nanoprism substrate and (2) the linear arrangement of the resulting islands. The first point is important because it may help to distinguish synthetic factors influencing Pt reduction pathways that result in either deposition onto Au NP substrates (in either dendritic or core–shell modes) or formation of frame-like architectures via GRR mechanisms. The second point indicates an exclusively bottom-up route for generating metal NP assemblies directly on colloidal NP substrates.

First, to elucidate factors influencing the reduction pathway of Pt(IV), we analyzed two synthetic parameters: Pt speciation and the ratio of Pt precursor to reducing agent. Because hydroxo substitution has been shown to increase the reduction potential of $[PtCl_6]^{2-}$ complexes,[31] differences in Pt speciation likely impact the reduction pathways of the metal ion precursor in NP syntheses (i.e., Pt(IV) reduction by addition of a reducing agent or by oxidation of the metal seed particle). In addition, as mentioned previously, the aqueous substitution of chloride ligands in CPA is well-known to be sensitive to time, temperature, light, complex concentration, and pH.[16] In order to study the influence of this speciation on NP formation, we induced Pt hydrolysis by addition of NaOH to the metal precursor solution (10 mM CPA, 4000 ppm). We used and analyzed all solutions within 3 h of preparation, and all solutions were protected from light (speciation was approximately constant over the time scale of our experiments; Figures S8 and S9). In aqueous solution at room temperature, the following reactions are representative of the speciation process at 10 mM CPA:

$$[PtCl_6]^{2-} + H_2O \rightleftharpoons [PtCl_5(H_2O)]^- + Cl^-$$

$$[PtCl_5(H_2O)]^- + H_2O \rightleftharpoons [PtCl_4(H_2O)_2] + Cl^-$$

$$[PtCl_5(H_2O)]^- \rightleftharpoons [PtCl_5(OH)]^{2-} + H^+$$

$$[PtCl_4(H_2O)_2] \rightleftharpoons [PtCl_4(OH)(H_2O)]^- + H^+$$

Keeping the age and concentration of the solution constant, we monitor pH-dependent ligand substitution using ^{195}Pt NMR spectroscopy in order to use well-defined Pt precursors in subsequent synthesis steps. Pt(IV) complex populations in the absence of NaOH (solution pH 1.8) consist of approximately 64% $[PtCl_4(H_2O)_2]$, 30% $[PtCl_6]^{2-}$, and 6% $[PtCl_5H_2O]^-$ (Figure 2, Table S3). At pH 3.2, the relative concentration of $[PtCl_6]^{2-}$ increases from 30% to 37%, and there is both a downfield shift and peak broadening, corresponding to a monosubstituted Pt(IV) species. These trends indicate a mixed population of OH^-- and H_2O-monosubstituted species. In the case of fast exchange (on the order of 10^{-5} s or faster), the chemical shift of the monosubstituted complex is a weighted average of the OH^-- and H_2O-substituted species.[18,32] Assuming that the observed chemical shift is due to this exchange process,

dx.doi.org/10.1021/ja504294p | J. Am. Chem. Soc. 2014, 136, 7873–7876

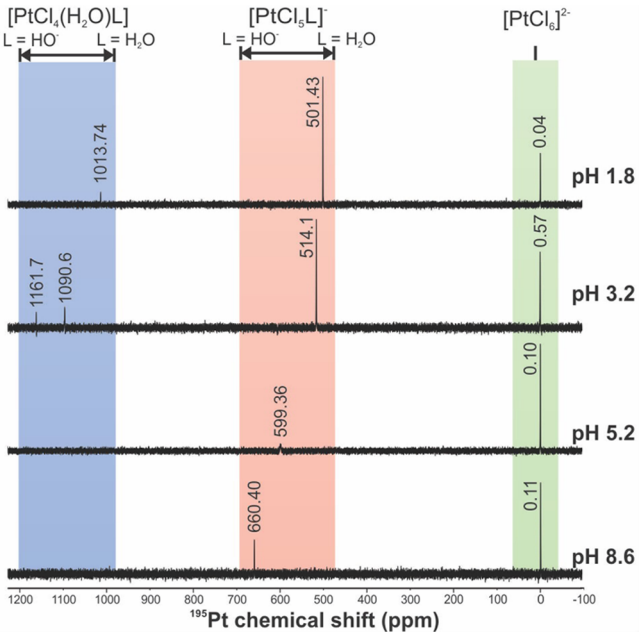

Figure 2. ^{195}Pt NMR analysis of CPA speciation as a function of pH. Chemical shift assignments for $[PtCl_6]^{2-}$ and the monosubtituted species were confirmed with $^{35/37}$Cl isotopologue distribution analysis (Table S3). For the monosubstituted (pink) and disubstituted complexes (blue), the peak position in ppm reflects the weighted average of H_2O- and OH-substituted species. Concentrations for each species as determined by signal integration are listed in Table S1.

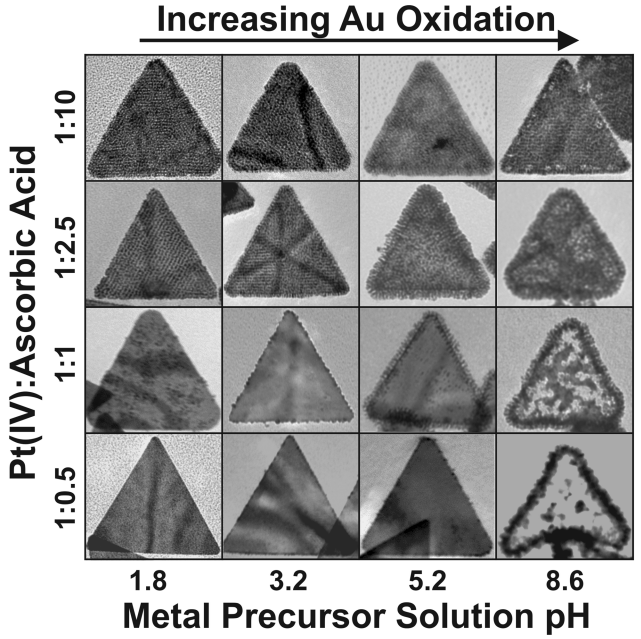

Figure 3. Comparison of nanoparticle morphologies as a function of Pt(IV):AA concentrations and metal ion precursor solution pH. See SI for supplementary TEM, UV-vis-NIR spectra, and STEM-EDS analysis of the NPs pictured (Figures S10–S15).

approximately 7% of the monosubstituted species is due to OH^- coordination (weighted average analysis from known chemical shift values, $[PtCl_5(H_2O)]^-$ = 501 ppm and $[PtCl_5(OH)]^{2-}$ = 660 ppm, as well as $^{35/37}$Cl isotopologue analysis, see SI). Using the same analysis at pH 5.2, approximately 20% of the Pt species are coordinated to OH^-, and the concentration of $[PtCl_6]^{2-}$ nearly doubles (from 37% to 70%). At pH 8.6, populations of the Pt complexes were measured as a 1:2 ratio of $[PtCl_5(OH)]^{2-}$:$[PtCl_6]^{2-}$ (33% and 67%, respectively). Interestingly, at pH 5.2 and above, no disubstituted complexes ($[PtCl_4L_2]^{n-}$; where L = OH^- or H_2O, n = 0, 1, or 2) were observed, and the majority of monosubstituted complexes contained a OH^- ligand, consistent with what may be expected from rising concentrations of OH^- and also in agreement with literature precedent.[16,18]

Using these data, the pH of Pt precursor solutions can be correlated with Pt(IV) speciation and ultimately correlated to different NP outcomes (Figure 3). When the pH of Pt(IV) precursor solution is low, reduction of the metal cation occurs primarily via AA oxidation, as evidenced by lack of oxidation in the nanoprism substrate. As pH increases, the concentration of $[PtCl_5(OH)]^{2-}$ also increases and oxidation of the Au particle begins to appear. These results are consistent with previous electrochemical studies of $[PtCl_6]^{2-}$ in water, which show that OH^--substituted complexes are more easily reduced.[31] Our results are consistent with these findings, where GRR-like products are observed only at increased populations of $[PtCl_5(OH)]^{2-}$ (e.g., pH 5.2 and 8.6), indicating that $[PtCl_5(OH)]^{2-}$ is a more aggressive oxidant.

We can further examine the impact of this Pt speciation by modulating the molar ratio of Pt(IV):AA (a traditional means of controlling the extent of NP growth). When the Pt precursor pH is held constant, the particle products follow well-known NP synthesis trends. For example, as the molar ratio of metal ion to reducing agent is increased, we observe a decrease in metal deposition onto the prism substrate (i.e., moving down a column in Figure 3). Conversely, when we hold the ratio of Pt(IV):AA constant and increase only the pH of the Pt precursor solution, the impact of Pt speciation is consistent with a progression toward GRR-mediated Pt reduction (moving across a row, Figure 3). The two competing Pt reduction pathways can be most clearly observed at pH 8.6 (also the highest observed concentration of $[PtCl_5(OH)]^{2-}$). At this pH, Pt(IV) reduction by oxidation of the nanoprism substrate competes effectively with reduction by AA at a scale that is observable across all ratios of Pt(IV):AA tested. At low ratios of Pt(IV):AA, this oxidation results in the formation of "pores" in the prism surface in addition to linear Pt island formation. At higher Pt(IV):AA ratios, mixed-metal nanoframes are formed exclusively (Figure 3, bottom right, Figure S13 and Figure S15, STEM-EDS).

Insight into the role of Pt precursor speciation on Pt reduction pathways facilitated the study of a second key aspect of the syntheses: the formation of Pt islands in regular linear arrays. Conducting time-dependent formation studies, it was found that Pt islands form in linear paths during their initial growth, where new islands appear to "fill-in" lines across the prism surface (Figure S2). For these "pseudo-stellated" nanoprisms, Pt island rows are either arranged with respect to a single base of the triangular prism (~70% of NPs) or organized with respect to all three bases of the nanoprisms (~30% of NPs, Figure S16). In these "three-base" cases, each row appears to move inward toward the center of the prism, forming a pattern of concentric triangles of decreasing size. In all cases, row separation distances are 5.4 ± 0.7 nm, which is too large to result from the underlying crystal structure of the nanoprism (a_{Au} = 4.079 Å). Further, the broad faces of the nanoprism approach atomically flat, and so this growth pattern is also unlikely to be associated with surface step-edges or other defects.[24,25] Strain at the interface between island and substrate also has been shown to produce ordered island arrangements.[33] However, the island linearity, row spacing (~5

dx.doi.org/10.1021/ja504294p | J. Am. Chem. Soc. 2014, 136, 7873–7876

nm), and observed island growth patterns (i.e., a "fill-in" mechanism) do not match well with strain-induced ordering observed elsewhere. Therefore, we hypothesized that the linear arrangement of Pt NP islands may result from a supramolecular architecture formed by the organic ligand adsorbates[34,35] (here, cetyltrimethylammonium bromide, CTAB) on the nanoprism surface, which act as "templates" for the linear growth pattern.

We tested this hypothesis by changing the ligands adsorbed to the Au nanoprism surface prior to Pt deposition. For the synthesis of pseudo-stellated nanoprisms, nanoprism seeds are purified from excess CTAB and other reagents via extensive washing using centrifugation. The final nanoprisms are then suspended in pure water and used in subsequent Pt addition reactions. Here, we exchanged this CTAB coating for two different ligands: 11-amino-1-undecanethiol (AUT), which is a small molecule that should form a relatively dense ligand layer, and poly(ethylene glycol) methyl ether thiol (PEGSH, M_n = 900 Da), which forms a random coil in solution and should produce a less dense ligand shell. After purification from excess thiolated ligands, exchange was confirmed by ^{1}H NMR and X-ray photoelectron spectroscopy (XPS) measurements (Figures S17−S19). Both AUT- and PEGSH-coated Au nanoprisms exhibited secondary metal deposition patterns markedly different than those observed for the CTAB-functionalized nanoprisms. For both AUT- and PEGSH-functionalized nanoprisms, Pt deposition was primarily observed on the sides of the particles (where one may expect some defects in molecular ligand coatings) and with no regular deposition morphologies (Figure S20). It is important to note that there is no added CTAB in the deposition step for any of the Pt deposition experiments, so the influence of the ligands (whether CTAB or others) is likely mediating a heterogeneous nucleation step.

In summary, these results highlight Pt speciation as a critical parameter in Pt-containing NP synthesis and should provide guidance in the development of new Pt-containing NP syntheses as well as clarify observations in existing strategies. For example, these mechanistic insights facilitated the investigation of NP deposition patterns as a function of organic ligands on the surface of the nanoprisms and may indicate a new method for controlling the pattern of secondary metal deposition onto NP substrates. Ultimately, the combination of metal precursor speciation and seed particle surface chemistry should be powerful tools for the synthesis of a wide variety of highly tailored multimetallic substrates with applications ranging from therapeutics to catalysis.

■ ASSOCIATED CONTENT

Ⓢ Supporting Information

Complete nanoparticle synthesis and characterization methods. This material is available free of charge via the Internet at http://pubs.acs.org.

■ AUTHOR INFORMATION

Corresponding Author

jem210@pitt.edu

Notes

The authors declare no competing financial interest.

■ ACKNOWLEDGMENTS

This work was supported by a National Science Foundation CAREER Award (CHE-1253143) and the University of Pittsburgh.

■ REFERENCES

(1) Greeley, J.; Mavrikakis, M. *Nat. Mater.* **2004**, *3*, 810.
(2) Chen, C.; Kang, Y.; Huo, Z.; Zhu, Z.; Huang, W.; Xin, H. L.; Snyder, J. D.; Li, D.; Herron, J. A.; Mavrikakis, M.; Chi, M.; More, K. L.; Li, Y.; Markovic, N. M.; Somorjai, G. A.; Yang, P.; Stamenkovic, V. R. *Science* **2014**, *343*, 1339.
(3) Cortie, M. B.; McDonagh, A. M. *Chem. Rev.* **2011**, *111*, 3713.
(4) Ghosh Chaudhuri, R.; Paria, S. *Chem. Rev.* **2011**, *112*, 2373.
(5) Chen, A.; Holt-Hindle, P. *Chem. Rev.* **2010**, *110*, 3767.
(6) Greeley, J.; Nørskov, J. K.; Mavrikakis, M. *Annu. Rev. Phys. Chem.* **2002**, *53*, 319.
(7) Cui, C.; Gan, L.; Heggen, M.; Rudi, S.; Strasser, P. *Nat. Mater.* **2013**, *12*, 765.
(8) Snyder, J.; Livi, K.; Erlebacher, J. *Adv. Funct. Mater.* **2013**, *23*, 5494.
(9) He, C.; Desai, S.; Brown, G.; Bollepalli, S. *Electrochem. Soc. Interface* **2005**, *14*, 41.
(10) Koenigsmann, C.; Wong, S. S. *Energy Environ. Sci.* **2011**, *4*, 1161.
(11) DeSantis, C. J.; Weiner, R. G.; Radmilovic, A.; Bower, M. M.; Skrabalak, S. E. *J. Phys. Chem. Lett.* **2013**, *4*, 3072.
(12) DeSantis, C. J.; Skrabalak, S. E. *J. Am. Chem. Soc.* **2012**, *135*, 10.
(13) Fan, F.; Liu, D.; Wu, Y.; Duan, S.; Xie, Z.; Jiang, Z.; Tian, Z. *J. Am. Chem. Soc.* **2008**, *130*, 6949.
(14) Lee, Y. W.; Kim, D.; Hong, J. W.; Kang, S. W.; Lee, S. B.; Han, S. W. *Small* **2013**, *9*, 660.
(15) He, W.; Wu, X.; Liu, J.; Zhang, K.; Chu, W.; Feng, L.; Hu, X.; Zhou, W.; Xie, S. *J. Phys. Chem. C* **2009**, *113*, 10505.
(16) Spieker, W. A.; Liu, J.; Miller, J. T.; Kropf, A. J.; Regalbuto, J. R. *Appl. Catal. A-Gen.* **2002**, *232*, 219.
(17) Mang, T.; Breitscheidel, B.; Polanek, P.; Knozinger, H. *Appl. Catal. A-Gen.* **1993**, *106*, 239.
(18) Shelimov, B.; Lambert, J.; Che, M.; Didillon, B. *J. Am. Chem. Soc.* **1999**, *121*, 545.
(19) Flynn, N. T.; Gewirth, A. A. *J. Raman Spectrosc.* **2002**, *33*, 243.
(20) Zhang, H.; Jin, M.; Wang, J.; Li, W.; Camargo, P. H. C.; Kim, M. J.; Yang, D.; Xie, Z.; Xia, Y. *J. Am. Chem. Soc.* **2011**, *133*, 6078.
(21) Schmid, G.; Lehnert, A.; Malm, J.; Bovin, J. *Angew. Chem., Int. Ed. Engl.* **1991**, *30*, 874.
(22) Yu, Y.; Zhang, Q.; Yao, Q.; Xie, J.; Lee, J. Y. *Chem. Mater.* **2013**, *25*, 4746.
(23) Millstone, J. E.; Wei, W.; Jones, M. R.; Yoo, H.; Mirkin, C. A. *Nano Lett.* **2008**, *8*, 2526.
(24) Millstone, J. E.; Park, S.; Shuford, K. L.; Qin, L.; Schatz, G. C.; Mirkin, C. A. *J. Am. Chem. Soc.* **2005**, *127*, 5312.
(25) Dahanayaka, D. H.; Wang, J. X.; Hossain, S.; Bumm, L. A. *J. Am. Chem. Soc.* **2006**, *128*, 6052.
(26) Mathur, A.; Erlebacher. *J. Surf. Sci.* **2008**, *602*, 2863.
(27) Villars, P.; Prince, A.; Okamoto, H. *Handbook of Binary Alloy Phase Diagrams*; ASM International: Materials Park, OH, 1995.
(28) Grzelczak, M.; Pérez-Juste, J.; García de Abajo, F. J.; Liz-Marzán, L. M. *J. Phys. Chem. C* **2007**, *111*, 6183.
(29) Lim, B.; Jiang, M.; Camargo, P. H.; Cho, E. C.; Tao, J.; Lu, X.; Zhu, Y.; Xia, Y. *Science* **2009**, *324*, 1302.
(30) Zheng, Z.; Tachikawa, T.; Majima, T. *J. Am. Chem. Soc.* **2014**, *136*, 6870.
(31) Hubbard, A. T.; Anson, F. C. *Anal. Chem.* **1966**, *38*, 1887.
(32) Levitt, M. H. *Spin Dynamics: Basics of Nuclear Magnetic Resonance*, 2nd ed.; John Wiley & Sons: West Sussex, UK, 2008.
(33) Brune, H.; Giovannini, M.; Bromann, K.; Kern, K. *Nature* **1998**, *394*, 451.
(34) Manne, S.; Cleveland, J. P.; Gaub, H. E.; Stucky, G. D.; Hansma, P. K. *Langmuir* **1994**, *10*, 4409.
(35) Liu, X.; Yu, M.; Kim, H.; Mameli, M.; Stellacci, F. *Nat. Commun.* **2012**, *3*, 1182.